Mechanical properties are tuned during development with the fibrous network nature of the Arabidopsis cell wall

Si Chen[a,b,c], **Isabella Burda**[a,c,d,e], **Purvil Jani**[f], **Bex Pendrak**[a,b], **Meredith N. Silberstein**[a,b,✉], **and Adrienne H.K. Roeder**[a,c,d,✉]

[a]Engineered Living Materials Institute, Cornell University, Ithaca, NY 14853, USA
[b]Sibley School of Mechanical and Aerospace Engineering, Cornell University, Ithaca, NY, USA
[c]Weill Institute for Cell and Molecular Biology, Cornell University, Ithaca, NY 14853, USA
[d]Section of Plant Biology, School of Integrative Plant Science, Cornell University, Ithaca, NY 14853, USA
[e]Genetics, Genomics, and Development Graduate Program, Cornell University, Ithaca, NY 14853, USA
[f]School of Chemical and Biomolecular Engineering, Cornell University, Ithaca, NY 14853, USA.

Plant organ growth involves significant deformation of cell walls, with the mechanical behavior of these walls, particularly the epidermal cell walls, playing a crucial role in plant morphogenesis. To gain insights into the mechanics of plant growth, it is vital to study and quantify the large-deformation mechanical properties of the epidermal cell walls in the context of development. To this end, we investigated the mechanical response of the Arabidopsis leaf epidermis to stretching. The epidermis exhibited a non-linear stiffening behavior that naturally fell into three regimes. Each regime also corresponded with distinct nonlinear behaviors in terms of transverse deformation (i.e., Poisson effect) and unrecoverable deformation (i.e., plasticity). We found that these properties arise not from the geometric structure of the epidermal cells but rather from the cell wall material, which behaves as a fibrous network material. Using a five-beam model, we demonstrated that these nonlinear behaviors result from the transition from reorientation and bending-dominated to stretch-dominated deformation modes of cellulose microfibrils. We further explored how these mechanical properties change during development and found stiffening behavior is more pronounced at later developmental stage. Finally, our investigation into the *spr2-2* mutant with altered morphology shows that it has anisotropic mechanical properties, likely contributing to the leaf curvature. Our finding reveals the fibrous network nature of cell walls, which gives a high degree of tunability in mechanical properties, allowing cells to adjust these properties to support the proper formation of plant organs.

Arabidopsis thaliana **plant | epidermis | nonlinear mechanical properties | plant development**

Correspondence: ***meredith.silberstein@cornell.edu; ahr75@cornell.edu***

Significance Statements

Plant organ growth involves significant deformation of cell walls, yet the large-deformation mechanical behavior of these walls in the context of development remains poorly understood. In this study, we stretched the leaf epidermis of a model plant to large deformation and found that its cell walls exhibit nonlinear mechanical behavior like fibrous network materials. We investigated how these mechanical properties vary across developmental stages and change in mutant plants with altered morphology, and explored possible mechanisms underlying these variations. Our finding suggests cell walls have a high degree of tunability in their mechanical properties, allowing cells to adjust these properties to support proper plant organ formation.

Introduction

Recent studies have highlighted the critical roles that mechanics play in plant growth and morphogenesis (1–7). Growth of plant organs involves significant deformation of cell walls, which depends on their mechanical properties across a large deformation range (8–10). The cells in the outermost layer, the epidermis, usually have thicker and stiffer cell walls, serving as a mechanical growth constraint against inner cells and playing a crucial role in plant morphogenesis (11, 12). However, the large-deformation mechanical behavior of epidermal cell walls, particularly in the context of development, is not well understood. Gaining this knowledge provides great potential for understanding plant growth and morphogenesis. In addition, these insights are crucial for developing living materials with programmed geometries and physical properties directly from plants (13–15).

Arabidopsis thaliana, a key model organism in plant development, has been extensively used to understand plant development from genetic and biochemical perspectives (16). However, the knowledge of large-deformation mechanical properties of Arabidopsis cell walls is limited. Two types of mechanical tests are commonly used to measure mechanical properties of plants (17, 18): 1) indentation-based tests, where an indenter is used to poke the sample while measuring the force and displacement (19); 2) tensile tests, which involve stretching the sample and monitoring force and deformation changes (20–22). Most mechanical tests done on Arabidopsis are indentation tests due its feasibility on small size samples (23, 24). However, there are concerns about how accurately these tests relate to in-plane mechanical properties, which are particularly relevant for growth (10, 18, 25). In addition, indentation tests often require assumptions, such as mechanical behavior of the cell wall or the cell geometry, to interpret the data, which may influence the reliability of the results (26, 27). In contrast, tensile tests can directly determine mechanical properties such as stiffness, Poisson's ratio, anisotropy, and plasticity without complex interpretive

DRAFT

processes. However, few tensile tests have been done on Arabidopsis plants (28–31), and these tests have several limitations: 1) They are typically performed at the organ scale, like hypocotyl or stem, making it difficult to relate the results to cell wall properties due to the complex geometry of cell patterning. 2) They usually focus on small deformation regions. However, the importance of understanding nonlinear mechanical behavior across a large deformation regime has recently been recognized (25, 32). 3) Existing studies typically focus on the relationship between deformation in the loading direction and force, neglecting resulting deformation in other direction. This additional information is also crucial for understanding the microstructure and deformation mechanisms of the cell. 4) These tensile properties are not well understood within the context of plant development. Onion epidermal cell walls are commonly used to study tensile mechanical properties because the specimen preparation procedure is well established (20–22, 25, 32). However, it is unclear whether these walls are still actively growing, and they may not fully represent typical growing cell walls. Therefore, it might be difficult to relate their mechanical properties directly to growth.

To address these limitations, we isolated an epidermal layer from the Arabidopsis leaf, which gives us a relatively simple geometry compared to the whole organ. We further improved the micromechanical tensile testing technique coupled with confocal microscopy recently developed for small-scale samples (30, 31), by utilizing Digital Image Correlation (DIC). This allowed us to automatically track markers on images and obtain accurate deformation measurements in all in-plane directions (33). We investigated the mechanical behavior of the leaf epidermis across a large deformation regime and explored the mechanisms controlling these behaviors. We also examined how these mechanical properties change during development, the underlying mechanisms, and their relation to growth. Additionally, we explored the mechanical properties of the mutant *spr2-2* with altered microtubule dynamics, the mechanisms behind these changes, and their relation to phenotype.

In this study, we showed that the Arabidopsis leaf epidermis exhibits a non-linear stiffening behavior that naturally fell into three regimes. Each regime also corresponds to distinct nonlinear behaviors in terms of transverse deformation (i.e., Poisson effect) and unrecoverable deformation (i.e., plasticity). Using finite element simulations based on the epidermal cell geometry, we found that these properties arise not from the geometric structure of the epidermal cells, but rather from the cell wall material itself. To further explore the underlying mechanisms of cell wall behavior, we adapted a five-beam model, suggesting that these nonlinear behaviors result from the transition of cellulose microfibrils from reorientation and bending-dominated to stretch-dominated deformation modes. This highlights the role of the cell wall as a fibrous network material. We observed that mechanical properties vary during development, likely due to changes in the connections between cellulose microfibrils. Additionally, the *spr2-2* mutant exhibited anisotropic mechanical properties, in contrast to the isotropic behavior of the wild type, which is likely linked to the enhanced alignment of cellulose microfibrils. This study suggests that the fibrous network nature of cell walls provides a high degree of tunability in their mechanical properties, which allows cells to adjust these properties to support proper plant organ formation.

Results

Nonlinear mechanical behavior of leaf epidermal cell layers. During growth, the cell wall undergoes tremendous deformation. To explore the mechanical properties associated with such a large deformation range, we stretched the epidermal peels of leaves from Arabidopsis (Figure 1A) using a tensile stage (Figure 1B). Each peel has one layer of abaxial (bottom side of the leaf) epidermal cells (Figure S1) which we cut into a thin rectangular strip for testing (Figure 1A). To accurately quantify the force and deformation of the epidermal peel test samples, we conducted the tensile tests on a confocal microscope to optically measure deformation by tracking fluorescent beads (34) coating the outside of the tissue (Figure 1B-C, Movie S1).

To understand how the epidermal tissue resists deformation under stretching, we performed a monotonic tensile test, in which the sample was stretched at a constant rate until it failed. The membrane force (force divided by the width of the sample) versus axial stretch (deformed length of the sample divided by the initial length of the sample) curve reveals three regimes (Figure 1D). To determine the stiffness in these regimes, we examined the tangent stiffness (slope of the membrane force versus axial stretch) (Figure 1E). In regime I, the sample is relatively soft, with a nearly constant low level of stiffness ($\sim$ 12 N/m). Then in regime II, the stiffness gradually increases as the stretch increases, exhibiting a nonlinear strain-stiffening behavior. This mechanical behavior suggests that more "elements" within the sample are becoming active in resistance to the loading. Finally, in regime III, the tissue is relatively stiff, with a nearly constant tangent stiffness ($\sim$ 70 N/m) (Figure 1D-E). Thus, the force and the deformation of the tissue do not have a simple linear relationship, which suggests a complex relation between turgor-driven growth and turgor pressure. This complexity cannot be simply represented by a single stiffness value derived from a limited range of deformation but rather should be characterized as a function that varies with deformation.

When a material is stretched, it will not only deform in the direction of applied force (in axial direction), but also in the transverse direction (Poisson effect); the relation between the deformation in both directions gives insight into the microstructure. In addition, knowing Poisson effect is important to relate mechanical response to multi-direction in-plane loading (e.g., equibiaxial), which is experienced by the cell wall of a growing cell since turgor pressure stretches the cell wall in all directions. To understand more about the Poisson effect of the epidermal peels, we looked at the deformation in both axial and transverse directions.

The transverse stretch (deformed width of the sample divided

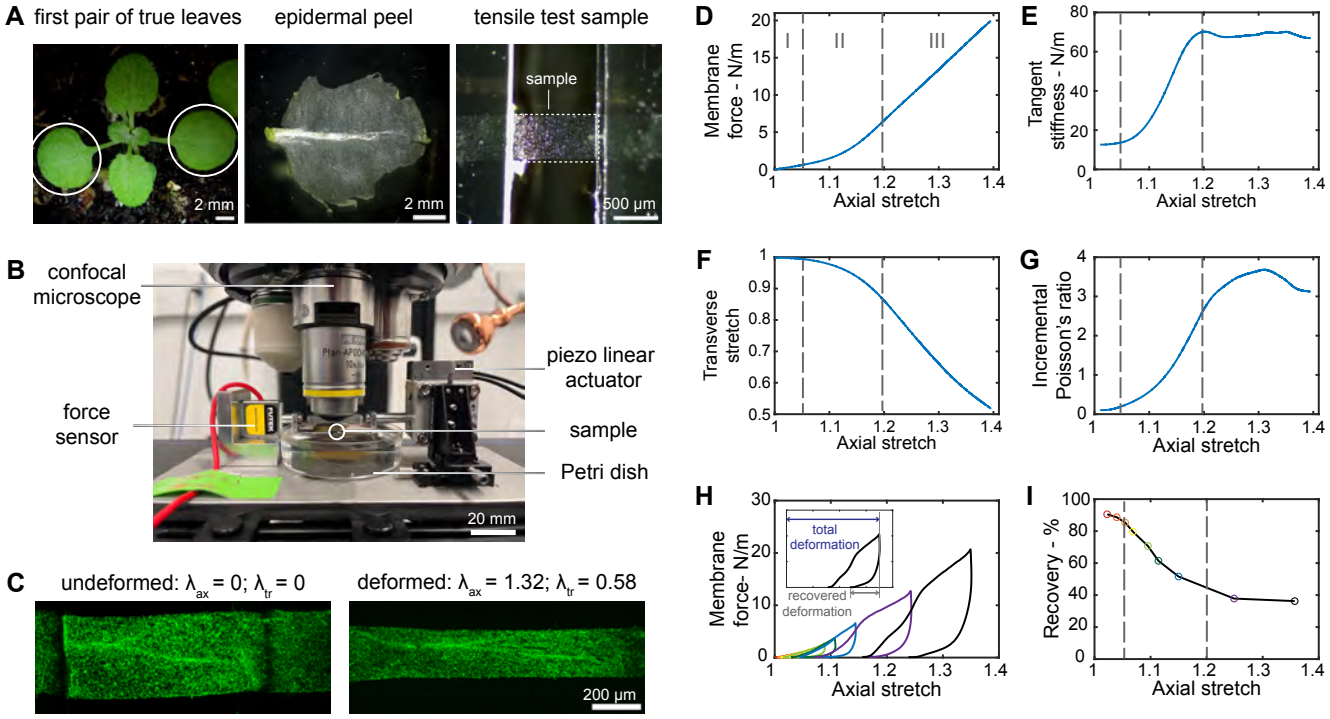

Fig. 1. Arabidopsis leaf epidermal peels have three-regime nonlinear mechanical behavior. (A) Test samples from epidermal peels of the first pair of true leaves. (B) Micromechanical tensile stage coupling with confocal microscopy. (C) Confocal images of a sample at undeformed and deformed status, λ_{ax} as the axial stretch, λ_{tr} as the transverse stretch. Representative (D) membrane force – axial stretch curve, (E) tangent stiffness – axial stretch curve, (F) transverse – axial stretch curve, and (G) incremental Poisson's ratio – axial stretch curve from monotonic tensile tests. Representative (H) membrane force – axial stretch curve and (I) Recovery – axial stretch from incremental cyclic tensile tests with loading-unloading cycles are distinguished by different colors. The recovery percentage is the percentage of recovered deformation relative to the total deformation. Regimes I, II, and III are divided by the dashed lines.

by the initial width of the sample) decreases (i.e., contracts) in a nonlinear manner as the axial stretch increases, which also corresponds to the three regimes previously identified (Figure 1F). To quantify the relation between the transverse stretch and axial stretch, we calculated the incremental Poisson's ratio (Methods). An incremental Poisson's ratio of 1 here implies conservation of surface area such that the increase in length is directly compensated by a decrease in width. In regime I, the transverse contraction is limited. The incremental Poisson's ratio is smaller than 1 and increases weakly with stretching, indicating that the area of the specimen is increasing. In regime II, the transverse contraction intensifies, and the Poisson's ratio increases and eventually is more than 1, which means that there is more transverse contraction than axial extension so that the area of the specimen is decreasing. In regime III, the transverse contraction stabilizes, and the Poisson's ratio increases but with a declining rate, reaches a peak, and then decreases as axial stretch increases further (Figure 1F-G). This unusual nonlinear Poisson effect distinguishes epidermal tissue from classical soft materials, such as rubbers, which typically have an incremental Poisson's ratio of 0.5 throughout deformation. An important question raised here is what underlying structure within the epidermal peels contributes to a large change in Poisson's ratio, which we will address in the next section.

The growth of a cell is due to irreversible deformation of the cell wall. To understand the underlying mechanism of irreversible (plastic) deformation, it is important to look at how this deformation evolves during stretching. We explore irreversible deformation by incremental cyclic tensile tests, in which the sample was loaded and unloaded (stretched and unstretched) cyclically with progressively increasing load levels until it failed. In each load-unloading cycle, the axial stretch at zero force point of the unloading curve is always larger than the immediately prior loading curve, indicating that irreversible deformation accumulates during stretching (Figure 1H). When the applied force exceeds the maximum force previously applied in incremental cyclic test, the membrane force versus the axial stretch response (Figure 1H) follows the response from the monotonic tensile tests (Figure 1D). To quantify how much deformation that is recoverable during stretching (the ability to return back to the original size), we calculated the recovery percentage (Figure 1I). The recovery versus axial stretch curve also exhibits a three-regime behavior. Most of the deformation (more than 80%) is recoverable in regime I, the recoverable deformation sharply decreases from 80% to 40% in regime II, and then eventually levels off in regime III. This aligns with the widely held view that the cell wall becomes plastic (yields) when the stress (stretch) passes the yield point (10). In addition, epidermal tissue becomes increasingly plastic with continuous stretching. This observation raises the question of what underlying mechanisms control the gradually changing plastic behavior of the epidermal tissue.

In summary, our comprehensive examination of the mechanical behavior of the epidermal peel reveals that it displays

nonlinear strain-stiffening, nonlinear Poisson effect, and nonlinear plasticity, all with the same three distinct regimes. This suggests that a common underlying mechanism governs these properties, which we will explore further in the next section.

Nonlinear mechanical behavior comes from the cell wall - a fibrous network material. The nonlinear mechanical behavior of epidermal peels can likely be attributed to a combination of two aspects: the cellular structure (shapes and arrangement of cells in the layer) and the material composition of the cell wall. We will first delve into whether and how the cellular structure influences the overall mechanical behavior of the epidermal peel. To explore the contribution of the cellular structure to the stiffness and Poisson effect, we utilized the finite element method to compare the mechanical responses of the cellular structure with the mechanical response of a single flat plate under stretch, representing just the intrinsic properties of the cell wall (Movie S2-3). We constructed cellular structures of the epidermal cells of the first pair of true leaves in silico (Figure 2A), as described in Methods. The top and bottom periclinal cell walls were treated as flat plates since the cells were deflated after peeling. The anticlinal walls were extruded from the cell outline boundary by the thickness of the cell which is 10 microns (Figure 2B). The same purely elastic mechanical properties are assigned to the material of the plate and cellular structure (Methods). Comparing the cellular model with the flat plate model, we find that the membrane force – axial stretch curves are very similar for these two models (Figure 2C). The two force-stretch curves have a maximum 8.3% deviation, indicating that the geometry of cellular structures is only a minor factor in the force deformation response. Further, the cellular structure is not responsible for the non-linear strain stiffening observed experimentally. Likewise, the axial–transverse stretch curves of the cellular structures are very close to that of a single plate with a maximum 0.4% deviation (Figure 2C), indicating that the cellular structure has almost no impact on the Poisson effect. The Poisson's ratio is not affected because there is no component of this cellular structure contributing to the lateral contraction. Varying the cell size of the cellular structure, the thickness of the cell wall, and the material model of the cell wall results in this same conclusion that the cellular structure has little impact on overall mechanical behavior (Figure S2). In other words, the nonlinear mechanical properties of the epidermal peels comes from the material of the cell wall.

Now the question is what underlying mechanisms control our observed nonlinear mechanical behavior of the cell wall. The cell wall consists of cellulose microfibrils embedded in a matrix of pectin and hemicellulose (10). Cellulose microfibrils contribute to the mechanical behavior in a manner that is strongly influenced by their orientation (1). We hypothesize that alignment of cellulose microfibrils during stretching leads to the nonlinear mechanical behavior of the cell wall. To examine this idea, we used cross-polarization microscopy to test the birefringence of the undeformed and samples deformed to an intermediate stretch (Methods). Cellulose microfibrils exhibit inherent birefringence (35), so the overall birefringence observed in the cell wall can provide insights into the orientation of these cellulose microfibrils within the cell wall. The similarity in overall brightness of the undeformed sample when oriented at 0 degrees and at 45 degrees suggests that the unstretched sample does not show birefringence other than the guard cells in which the cellulose microfibrils are highly aligned (Figure 2D). This observation implies that the cellulose microfibrils are initially distributed evenly in all orientations within the cell wall. In contrast, the deformed sample oriented at 45 degrees is brighter, whereas at 0 degree is not, indicating the stretched sample becomes birefringent. This change indicates that cellulose microfibrils orient towards the axial direction as a result of stretching (Figure 2E).

We first assess whether the alignment of microfibrils based on an affine deformation assumption can account for the mechanical behavior of the cell wall. We adapt a simple affine isotropic network model (36), in which all fibers are stretched and rotate such that local deformation is consistent with global deformation (Figure 2F; SI, Section A). The membrane force, tangent stiffness, transverse stretch, and incremental Poisson's ratio versus the axial stretch curves resulting from this affine assumption (Figure 2G) all show different trends compared to the experimental results (Figure 1D-G). This model predicts that the strain stiffening behavior has only two regimes instead of three regimes: stiffness gradually increases in regime I and levels out in regime II. In addition, this model predicts that the incremental Poisson's ratio increases monotonically instead of increasing until reaching a peak and then decreasing, as in the experimental data. Therefore, the nonlinear mechanical behavior of cell walls under stretch cannot be solely attributed to the reorientation of cellulose microfibrils resulting from affine deformation.

Two key aspects overlooked in the aforementioned affine model are that cellulose microfibrils can bend/unbend (37) in addition to stretch/unstretch (i.e., beam-like in mechanics terminology), and that these microfibrils can slide relative to one another, deforming and sliding through the amorphous matrix (1). Because of their large length-to-diameter aspect ratio, cellulose microfibrils close to the transverse direction tend to bend rather than shorten in length axially, which reduces the resistance to transverse deformation. To incorporate this bending under compression, we adapted a five-beam model (38, 39) utilizing a simple diamond structure of five beams (Figure 2H; SI, section A), which we use to conceptualize the arrangement structure of cellulose microfibrils in the cell wall. In this model, beam AB represents cellulose microfibrils close to the transverse direction; it undergoes bending if the structure is stretched along the indicated force direction. Beams AC, AD, BC, and BD then represent the majority of cellulose microfibrils, which rotate towards the direction of applied force and elongate elastically. The connector in our model, which we have added to the original five-beam concept, represents the links between cellulose microfibrils, which could be biomechanical hotspots, the pectin matrix, or hemicellulose (10). To capture the relative sliding of microfibrils within the cell wall causing plastic behavior

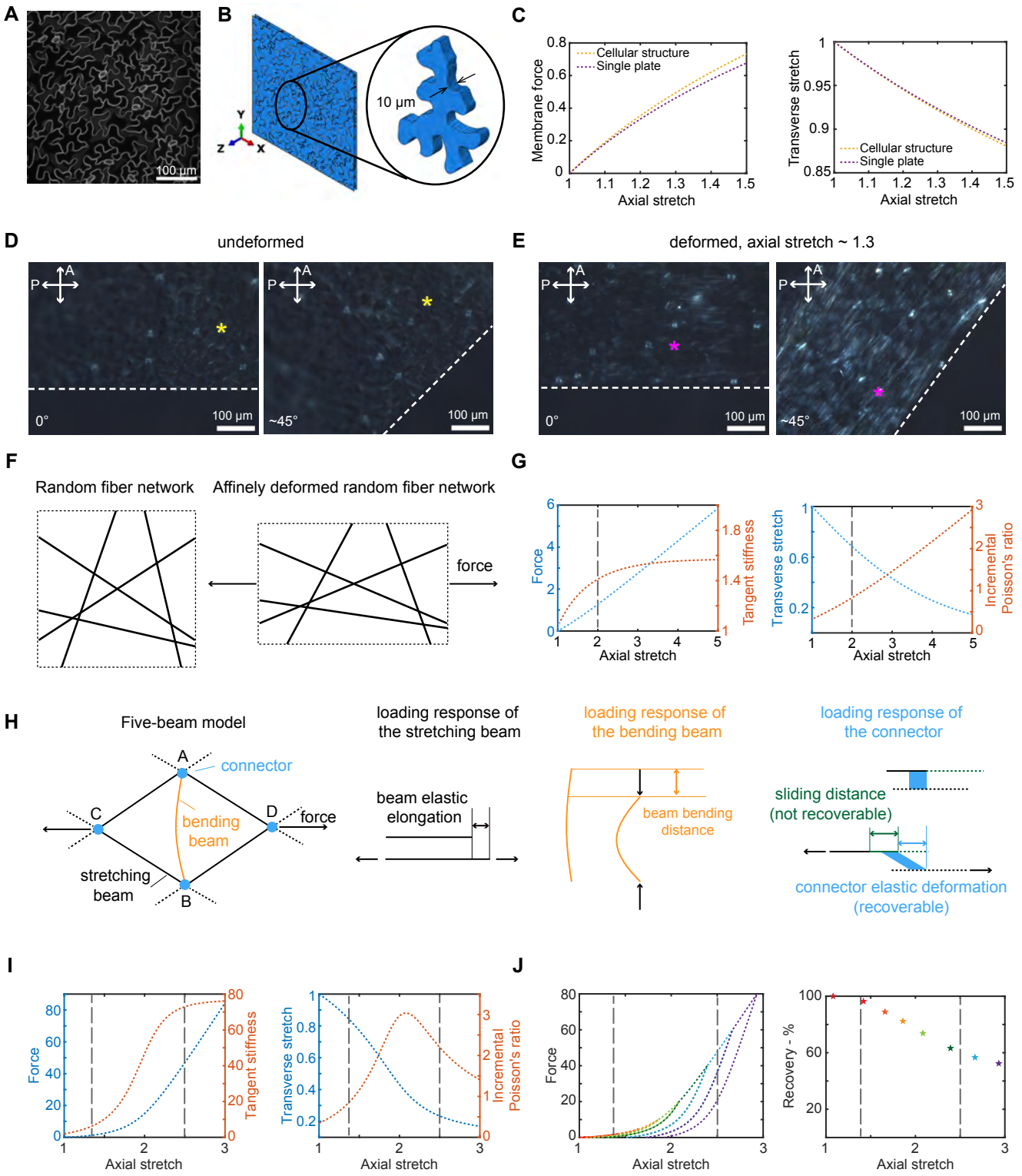

Fig. 2. Physical mechanisms that could be underlying the stress response of the epidermal peel to deformation. (A) Maximum projection of the confocal z-stack image of leaf abaxial side epidermal cells with the membrane marker, and based on it (B) the cellular structure of the epidermis is constructed in Abaqus. The inset shows an isolated cell, with two arrows indicating the thickness of the cell. (C) Membrane force versus axial stretch curves and Transverse stretch versus axial stretch curves of FEM simulation results of three cellular structures and a single plate. Cross-polarized microscope images at 0 and 45 degrees between the axial direction and polarizer of (D) an undeformed sample and (E) a deformed sample. The star marker indicates the same point of the sample oriented at different angles. (F) Schematic of the affine isotropic network model at undeformed and affine deformed status respectively. (G) Force (left axis) and tangent stiffness (right axis), and transverse stretch (left axis) and incremental Poisson's ratio (right axis) versus axial stretch curves of the affinely isotropic network model. (H) Schematic of the five-beam conceptual model and loading responses of stretching beam, bending beam and connector respectively. (I) Force (left axis) and tangent stiffness (right axis), transverse stretch (left axis) and incremental Poisson's ratio (right axis) versus axial stretch curves of monotonic loading, (J) force and recovery percentage versus axial stretch curves of loading-unloading of the five-beam conceptual model.

(1), we assume that if the force exceeds a certain threshold, the connector will not only deform but also slide between beams. Note that we are not comparing the exact values, as our model uses a simple geometry while the actual structure of cellulose microfibrils in the cell wall is much more complex - we aim to represent qualitative trends.

The membrane force, tangent stiffness, transverse stretch, and incremental Poisson's ratio versus the axial stretch curves for the five-beam model (Figure 2I) all show similar trends compared to experimental results (Figure 1D-G), exhibiting nonlinear mechanical behavior with three regimes. The recovery behavior of the model (Figure 2J) also shows a similar trend to the experiments, where the recovery gradually decreases with increased stretch (Figure 1H-I). From this five-beam model, the three characteristics of the cell wall's nonlinear mechanical behavior can be understood to result from the transition of the deformation mode of cellulose microfibrils from reorientation and bending-dominated to stretch-dominated. 1) Strain-stiffening behavior: the microfibrils close to the transverse direction tend to bend since it's energetically favorable initially, a small amount of force can deform the network, so the stiffness of the network is low; as the network deforms, the microfibrils close to the axial direction align and a larger force is needed to deform the network, so the stiffness of the network is gradually increasing; eventually, the angle of the side microfibrils stabilize so axial deformation dominates, and the stiffness of the structure reaches a plateau. 2) Poisson effect: as the microfibrils close to the transverse direction bend, it leads to more transverse contraction than if it were compressing axially, causing an increase in the Poisson's ratio. As the network deforms, it becomes harder to further bend the transverse microfibrils, which leads to a decrease in the incremental Poisson's ratio. 3) Irreversible deformation: when the bending mode dominates, the transmitted force between the microfibrils is relatively small resulting in minimal fiber-fiber sliding. As fiber stretching mode starts to dominate, the transmitted force gradually increases, resulting in more sliding, thus irreversible deformation. This implies that the transition of actions of cellulose microfibrils from reorientation and bending-dominated to stretch-dominated leads to the nonlinear stiffening and nonlinear Poisson effect of the cell wall, and also a gradual change in plasticity.

Mechanical properties of the cell wall change during development. During development, the correct formation of plant organs is ensured by properly coordinated growth rates, which are influenced by the mechanical properties of the cell wall. In this section, we will examine changes in the overall mechanical behavior of the cell wall during development and how these changes relate to growth rates. We will also discuss the possible mechanisms that control these alterations in mechanical behavior.

To investigate the mechanical behavior of the cell wall at various developmental stages with distinct growth rates, we conducted monotonic tensile tests on the epidermis of the first pair of true leaves at 12-day, 18-day or 25-day post-germination, corresponding to relatively fast growth, slow growth, and no growth respectively (Figure 3A). For reference, previous measurements in Figure 1 were made at 25 days. Leaf epidermises from all developmental stages show three regime strain-stiffening behavior as discussed before (Figure 3B). The stiffness E_1 in regime I (the slope of the initial linear regime) of samples at different stages are not significantly different, while the stiffness E_2 in regime III (the slope of the final linear regime) increases with high statistical significance as the samples get older. Therefore, growth rate is associated with the stiffness E_2 but not E_1, and a slower growth rate corresponds to a higher E_2. This result aligns with the widely held view that stiffness serves as an indicator of wall extensibility, which in turn controls the growth rate (40). Moreover, it is important to consider stiffness beyond regime I, as stiffness in this initial regime tends to remain consistent throughout development.

To determine how the Poisson's ratio changes over development, which provides insights into deformation mechanisms, we examined the transverse stretch versus axial stretch curves and found they are similar among different stages (Figure 3C). Additionally, there are no statistically significant differences in the initial incremental Poisson's ratio ν_1 and the peak Poisson's ratio ν_2 among these stages (Figure 3C).

To explore the plastic behavior at different developmental stages we conducted incremental cyclic tensile tests on leaf epidermal peels. The plastic behavior of samples from various developmental stages consistently shows three regimes: most deformation is recoverable in regime I, recovery decreases sharply in regime II, and levels off in regime III (Figure 3D). At the same stretch level, the recovery percentage of deformation is similar across different development stages. Interestingly, the membrane force versus residual stretch curves vary across these three stages: at the same load level the accumulated residual stretch is larger in earlier stages than in late stages. This result implies that when turgor pressure within cells increases, older cells tend to have less immediate plastic deformation.

To explore the possible mechanisms behind the variation in the stiffening behavior of cell walls at different stages, we revisit the five-beam model in the previous section. As we found previously, the mechanical properties of the epidermis come from the cell wall materials, whereas the cellular structures at these different developmental stages have little influence on the overall mechanical behavior (Figure S2). For fibrous network materials, factors such as fiber density, fiber orientation, and crosslinks between fibers can significantly influence the stiffness (38). We first consider the increase in fiber numbers due to more cellulose microfibrils being deposited into the cell wall as it grows. This, however, would scale E_1 and E_2 equally, contradicting the experimental results. Therefore, more deposited cellulose microfibrils cannot explain the stiffness variation. Additionally, more alignment of cellulose microfibrils in the proximal-distal directions during development is unlikely, since the mechanical behavior in both medial-lateral and proximal-distal directions are quite similar at all development stages (Figure S3). We

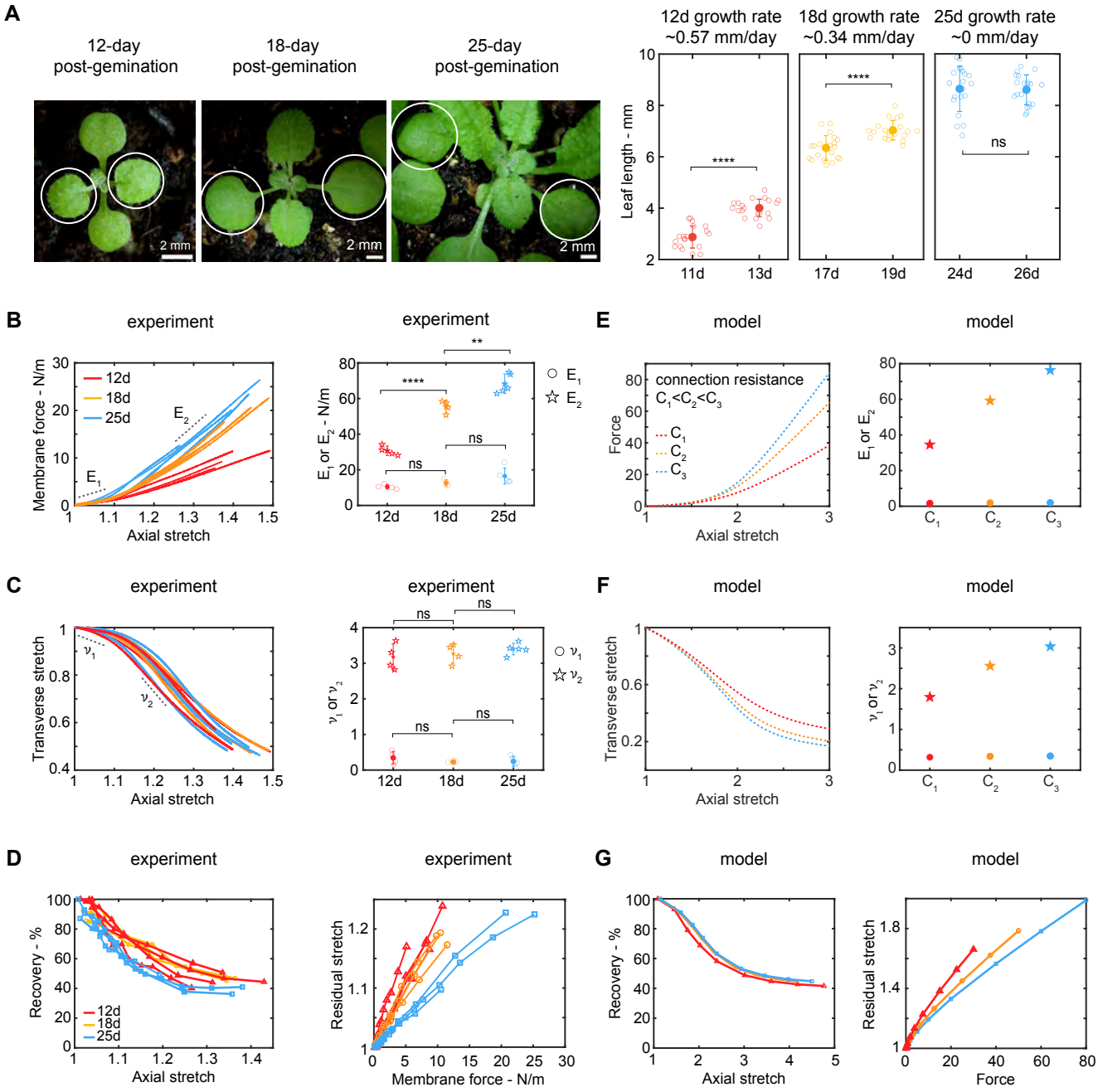

Fig. 3. Changes in the mechanical properties of leaf epidermis across developmental stages and potential underlying mechanisms: (A) First two true leaves of plants for three developmental stages (12, 18, and 25 days pot-germination) and their growth rates calculated based on leaf length measurements taken one day before and after each stage. (B) Mechanical force - axial stretch curves and scatter plot of the initial (E_1) and the final stiffness (E_2), (C) transverse – axial stretch curves, and scatter plot of the initial (ν_1) and peak Poisson's ratio (ν_2), (D) recovery percentage versus axial stretch curves and residual stretch versus membrane stress for 12-day (four curves), 18-day (three curves), and 25-day (three curves) stage from incremental cyclic tests. Note that one data from the 25-day stage is reused from Figure 1I. (E) Membrane force – axial stretch curves, and plot for the initial (E_1) and final stiffness (E_2), (F) transverse stretch – axial stretch curves, and plot for the initial (ν_1) and peak Poisson's ratio (ν_2), and (G) recovery percentage – axial stretch curves from the model by varying the deformation resistance of connectors. Statistics were performed by the two-sample two-tailed t-test.

then examine the impact of crosslinks by varying the connector deformation resistance of the five-beam model. The results show that the connector deformation resistance does not influence the initial slope of the force-stretch curve but significantly influences the later stiffening behavior (Figure 3E). A higher connector deformation resistance results in a high final stiffness E_2 but maintains a similar initial stiffness E_1. This is because the initial stiffness is dominated by bending and orientation of the fibers, while the final stiffness is dominated by the fiber stretch and slip. This suggests that the variations in stiffness at different stages may be primarily due to changes in the connections between cellulose microfibrils. The changes in the deformation resistance of the connector can also explain some of the trends in the Poisson effect and

plastic behavior of the cell walls at different stages. The changes in the deformation resistance of the connector do not affect the initial Poisson's ratio, aligning with experimental observations (Figure 3F). A higher resistance leads to an increased peak Poisson's ratio in the model, whereas experiments show this trend but without a significant difference. This discrepancy may be attributed to the simplified structure of the five-beam model, which does not fully represent the complexity of cellulose microfibrils in cell walls.

Exploring the same five-beam model for plastic behavior (Figure 3G), we found that the model accurately captures the similarity in recovery-stretch curves across different development stages. The model also shows that the residual stretch is smaller at the same force level for older development stages. This suggests that plastic behavior is dominated by stretch rather than force.

The anisotropy of the cell wall is affected by microtubules. During plant development, the regulation of anisotropic growth generates various organ shapes. It is generally accepted that this anisotropy is generated by the anisotropic mechanical properties of the cell wall (9). To investigate this relationship, we compared cell wall anisotropy between wild-type plants and a mutant with altered leaf shape. Given that microtubules guide the deposition of cellulose microfibrils in the cell wall and are closely associated with anisotropic mechanical properties (41), we selected a microtubule-related mutant, *spiral2* (*spr2-2*). A *spr2-2* mutant plant does not have functional SPR2 protein, which is a microtubule-associated protein that binds to the minus end of microtubules and stabilizes them (42–44). As a result, microtubules in this mutant are more dynamic which leads to more aligned/anisotropic microtubules in *spr2-2* than in wild-type Arabidopsis (45). In wild-type plants, the first pair of true leaves grow isotropically and form a flat circular blade (Figure 4A). However, in the *spr2-2* mutant, the first pair of true leaves are twisted and curl in a counterclockwise orientation (Figure 4A), implying altered cell wall anisotropy in this mutant. To test this hypothesis, we compare the cell wall anisotropy between the *spr2-2* mutant and wild-type plants and explore the possible mechanisms underlying alterations in mechanical behavior.

To investigate the difference in anisotropic mechanical behavior of the cell wall between *spr2-2* mutant and wild type, we conducted monotonic tensile tests on the epidermis of the first pair of true leaves at 12 days post-germination when the curled leaf phenotype begins to appear. We measured mechanical properties in four orientations: counterclockwise tilted 45 degrees relative to the midrib (ct), clockwise tilted 45 degrees relative to the midrib (t), proximal-distal (l), and medial-lateral (h) (Figure 4B). These orientations were chosen to provide a comprehensive assessment of anisotropy, examining mechanical behavior in axial, transverse and both diagonal directions relative to the main midrib axis of the leaf. Results of monotonic tensile tests show that samples from all four directions of both the mutant and wild type exhibit the same three-regime behavior (Figure S4). For the *spr2-2* mutant, the initial stiffness E_1 and initial Poisson's ratio ν_1 show no significant difference between ct and t or between l and h orientations. However, the final stiffness E_2 (the slope of the final linear regime) and peak Poisson's ratio ν_2 in the ct orientation are statistically significantly higher than in the t orientation, while in l and h orientation have no significant difference (Figure 4C-D). For wild type, there are no significant differences in the initial stiffness E_1, final stiffness E_2, initial Poisson's ratio ν_1 and peak Poisson's ratio ν_2 between ct and t orientations, or l and h orientations (Figure 4C-D). This indicates mechanical properties are anisotropic in *spr2-2* mutant, in contrast to the wild type, which are isotropic. This anisotropy of *spr2-2* likely originates from a slightly enhanced fiber alignment in the ct direction (given that E_2 in this direction is 40% greater than the t-direction) and likely contributes to leaf curvature.

The five-beam model offers insights into anisotropic mechanical behavior. To determine if fiber alignment can cause these anisotropic behaviors, we utilized the model again. For isotropic mechanical behavior, we used the same parameters with the angle parameter (θ_0) of the model as originally employed (SI, section B) in all directions to produce the same mechanical behavior (Figure 4E), setting it as the baseline. To examine how the preferential cellulose microfibrils orientation influences mechanical properties, we alter the angle θ between two stretching beams in the five-beam model (Figure 4F). We used a smaller angle parameter ($\theta_1 < \theta_0$) to represent the preferential cellulose microfibrils orientation along the stretching direction, and a larger angle parameter ($\theta_2 > \theta_0$) to represent the preferential cellulose microfibrils orientation perpendicular to the stretching direction. We found that the θ_1 case produces a similar initial stiffness E_1 but a significantly higher final stiffness E_2 than θ_0 case, whereas the θ_2 case produces a lower final stiffness E_2 than θ_0 case (Figure 4G). Additionally, the θ_1 small angle case produces higher ν_1 and ν_2 whereas θ_2 large angle case produces lower ν_1 and ν_2 compared to θ_0 case (Figure 4H). This indicates that the enhanced alignment of cellulose microfibrils in the cell wall of *spr2-2* is close to the ct direction, or in other words, nearly perpendicular to t direction, leading to observed anisotropic behaviors. We note that ν_1 is similar in all orientations in the experiments, which might be attributed to the simplicity of the five-beam model enhancing the sensitivity of ν_1 to the initial geometry.

Discussion and Conclusion

In this study, we investigated the mechanical behavior of the Arabidopsis leaf epidermis. We explored how mechanical properties change across a large deformation regime over different developmental stages. Our findings reveal that: 1) the leaf epidermis exhibits distinct three-regime nonlinear mechanical behavior, arising from the intrinsic deformation mechanisms of the cell walls, which are fibrous network materials; 2) mechanical properties vary across developmental stages associated with different growth rates, potentially due to changes in the connections between cellulose microfibrils; 3) the *spr2-2* mutant with curled leaves shows anisotropic

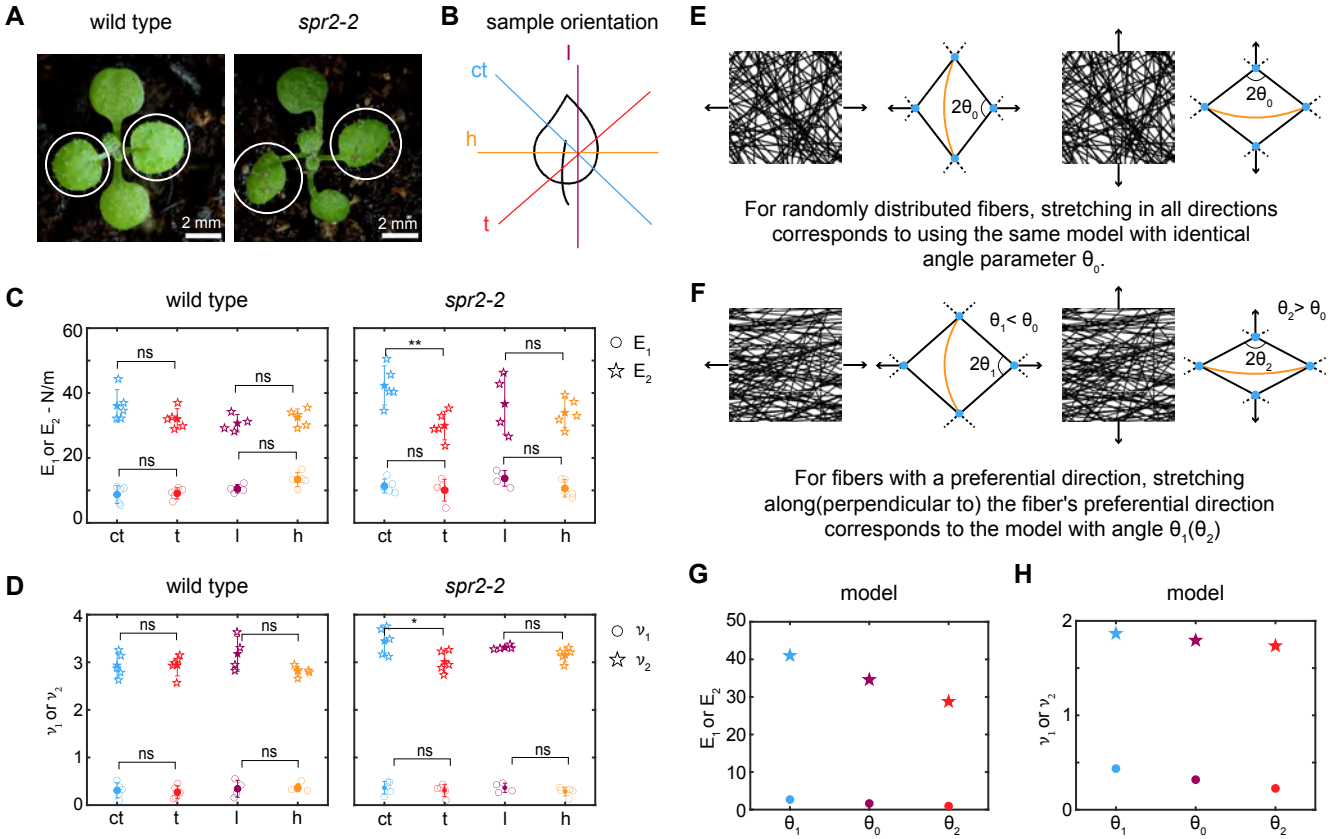

Fig. 4. *spr2-2* mutant shows anisotropic mechanical properties, implying enhanced alignment of cellulose microfibril. (A) first two true leaves of wild type and *spr2-2* mutant. (B) Preparation of the samples from the leaf epidermis in four orientations (l, h, ct and t). In the schematics, the peeled abaxial epidermis is in the normal orientation (cuticle side oriented away from the view). Scatter plot displaying (C) the initial (E_1) and the final stiffness (E_2) (D) the initial Poisson's ratio (ν_1) and the peak Poisson's ratio (ν_2) for four orientations of wild-type and *spr2-2* mutant samples. For the wild type: ct (five blue points), t (five red points), l (four purple points) and h (five orange points). For *spr2-2* mutant: ct (five blue points), t (five red points), l (four purple points), and h (five orange points). (E) Schematic of the five-beam model representing randomly distributed fibers under loading in both horizontal and vertical directions. (F) Schematic of the five-beam model with varying angles between two stretching beams, representing fibers with a horizontal preferential orientation under loading in horizontal and vertical directions. Scatter plot of (G) the initial (E_1) and the final stiffness (E_2), (H) the initial Poisson's ratio (ν_1) and the peak Poisson's ratio (ν_2) from the model with two different angles. Statistics were performed by the two-sample t-test.

mechanical properties, likely linked to the enhanced alignment of cellulose microfibrils.

The observed three-regime nonlinear strain-stiffening behavior, known as a J-shaped stress-strain curve, is typical of many soft mammalian biomaterials (46). This behavior allows animal tissues to undergo deformations within a range while preventing excessive deformation that could lead to damage when stress exceeds this range (47), and likely provides similar benefits for plant tissues. According to Laplace's law, slight turgor pressure changes can cause large deformations of plant cells if considering linear elasticity, but stiffening behavior could prevent this (SI, section C). This nonlinear stiffening has also been observed in other plant tissue, like apple fruit and potato tuber tissues, though it is unclear whether it comes from the tissue structure or individual cells, and the underlying mechanisms have not been extensively studied (48, 49). In contrast, the primary cell wall of the onion bulb, often examined for its mechanical properties, exhibits a different pattern where stiffening is typically followed by softening (25, 32). These differences highlight that the mechanical behavior of cell walls can vary between different organs and species. Additionally, it has been proposed that strain-stiffening behaviors can vary within different regions of the same organ, influencing growth patterns and organogenesis (50). The differences in mechanical behavior are worth further exploration.

There is less literature on the Poisson's ratio of plant tissues compared to stiffness measurements, and it is often treated as a constant, like 0.5, in interpreting indentation tests (19). To our knowledge, our work is the first to demonstrate how Poisson's ratio changes with stretch across a large deformation regime. Understanding Poisson's ratio is crucial not only for providing insight into deformation mechanisms, but also for analyzing the deformation of plant cells or tissues under complex loading conditions (SI, section D). For instance, in a pressurized cylindrical cell stretched along its long axis, knowing the Poisson's ratio is essential for calculating the cell's overall stiffness. A higher Poisson's ratio in the cell wall would make the cell more resistant to deformation (SI, section D.1, Case II). If Poisson's ratio increases with deformation, as observed in regime I, the cell becomes progressively more resistant, thereby reducing the impact of forces that come from neighboring cells or the environment. These concepts are extensible to large deformation, although more

information is needed to draw direct conclusions (SI, section D.2).

The plastic behavior observed here in Arabidopsis is also present similarly in onion bulb epidermal cell walls, where it results from the sliding of cellulose microfibrils (25). Notably, while this sliding leads to greater plastic deformation as the cell wall deforms, it does not necessarily weaken the cell wall in an Arabidopsis leaf. The strain-stiffening beyond the previous maximum load level is similar to that observed in monotonic tests. This combination of strain-stiffening with plastic deformation is known as hyperelastic-plastic behavior (51) and has been observed in physically crosslinked nanocellulose hydrogels (52), where it is explained by the breaking and reforming of physical crosslinks. This suggests that during sliding, the connections between cellulose microfibrils may temporarily disassociate and re-associate, maintaining the integrity of the cell wall.

The observed trends in these three mechanical behaviors suggest that the cell wall behaves like a fibrous network material. Fibrous network materials are characterized by fibers forming an interconnected network, with or without a matrix, where the overall behaviors emerge from the collective deformation of the fibers and their interactions (38). This is distinct from fiber-reinforced composites, where mechanical properties result from the additive contributions of both the matrix and the fibers (51, 53). Fibrous network materials encompass a broad range of materials, including nonwovens (54), mycelium (55), blood clots (56) and mammalian skin (57), all of which exhibit diverse mechanical behaviors. Notably, mammalian skin, a well studied living material, shares significant similarities with plant epidermal cell walls. Skins also have stiff fibers – collagen fibers - as their primary load-bearing elements, forming a complex three-dimensional network (58). Skin also exhibits a J-shape strain-stiffening behavior and a large Poisson effect when subjected to axial stretch (59), which comes from collective behavior of straightening, aligning and stretching of collagen fibers (60). This suggests a similar deformation mechanism happening in the cell walls. However, there are two key differences between mammalian skin and cell walls: 1) collagen fibers are more flexible than cellulose microfibrils, resulting in a more pronounced tortuosity in the collagen network; 2) sliding occurs between cellulose microfibrils, while collagen fibers have less sliding motion (58). These differences lead to slightly different mechanical behavior of skin compared to plant cell walls: 1) strain-stiffening is more pronounced in skin because collagen fiber straightening requires less force in the first regime, and the covalent crosslinks preventing sliding allows greater stiffening in the third regime; 2) the deformation in skin is mostly recoverable due to the covalent crosslinks between collagen fibers. Given the well-established research on skin mechanics, comparisons between two systems may offer valuable insights that could enhance our understanding of cell wall mechanics, which is worth exploring in future research.

The fibrous network structure of cell walls enables a high degree of tunability in their mechanical properties, allowing cells to adjust these properties to support the proper formation of plant organs. Our results indicate that as the leaf develops, the stiffness in the third regime increases, and the plastic deformation at the same stress level decreases. These changes are likely due to alterations in the connections between cellulose microfibrils, which may involve hemicellulose tethering, the pectin matrix and direct cellulose–cellulose contacts, with the last likely being the most influential (61). The coarse-grained physical model of epidermal cell walls (62) shows that strengthening cellulose-cellulose contacts increases wall stiffness and decreases plasticity while increasing the binding energies between cellulose and matrix polysaccharides has little effect. This suggests that the observed changes in mechanical properties during development are likely due to modifications in cellulose–cellulose contacts. Additionally, the orientation of cellulose microfibrils is another critical factor influencing mechanical properties. Our findings indicate that the *spr2-2* mutant exhibits anisotropic mechanical behavior, likely due to the enhanced alignment of cellulose microfibrils, while the wild type displays isotropic behavior.

Overall, our study highlights the intricate mechanical properties of the Arabidopsis leaf epidermis and underscores the importance of understanding the fibrous network nature of cell walls. This understanding could lead to new insights into the relationship between mechanical properties and plant morphogenesis.

Methods

Plant materials. *Arabidopsis thaliana* accession Col-0 plants were used as wild type, and the *spr2-2* (AT4G27060) mutant is in the Col-0 background (43, 45). Seeds were sown on Lambert Mix LM-111 soil and then kept at 4°C for two days. After stratification, seeds were transferred to a growth chamber; this event defines post-germination day 0. Plants were grown under long-day light conditions (16 hours light/8 hours dark). Temperature and humidity conditions in the growth chamber were maintained at 22°C and 50% RH respectively.

Leaf epidermal peel and tensile test sample preparation. The first pairs of true leaves were dissected from the plants. We used custom gelatin-coated cloth (SI, Methods) to separate the abaxial epidermal peel from the leaf (Figure S5A-B). Thin rectangular strips approximately 0.4 mm wide were cut from the epidermal peels at the desired orientation within the leaf. Each sample was immersed in a fluorescent bead suspension (Magsphere AMF-300, diluted 2.5 µL into 250 µL water) for 15 minutes, and then gently swirled in water to remove excess fluorescent beads before testing. The strips were then gripped at both ends using Gorilla Crystal Clear Tape, leaving an ungripped length (avoiding the midrib) of approximately 0.9 mm. Two strips of aluminum foil were used to prevent the sample from stretching (Figure S6A). Then, the sample with the gripped tape was attached to the custom micromechanical tensile stage using magnets (Figure S6B-C). The Petri dish was filled with water, and the

sample was placed on the water surface to maintain moisture and flatness. The aluminum foil strips were cut before testing.

Tensile test procedure. For the monotonic tensile test, the sample was stretched at a constant velocity of approximately 2.5 µm/s using the piezo linear stage until failure. The force exerted on the sample was monitored continuously by the load cell. Simultaneously, the pattern of fluorescent beads on the sample was captured continuously by a confocal microscope (Zeiss 710 upright laser scanning confocal microscope with a 10x lens) as time-series images at 1-second intervals. During testing, the confocal stage was manually adjusted to ensure the specimen remained in the center of the imaging window. For the incremental cyclic tensile test, the sample was initially stretched at a constant velocity of approximately 2.5 µm/s and then unloaded at the same velocity until the force reached zero. The sample was then reloaded beyond the previous maximum load level, and this cycle was repeated until failure. The force and images of the bead pattern were recorded in the same manner as in the monotonic tensile test.

Post-experiment analysis. The images of the fluorescent bead pattern were analyzed using commercial Digital Image Correlation software (Zeiss Inspect Correlate). Axial and transverse stretch data versus time were exported from the software. The width of the sample was measured from the confocal image of the undeformed sample using ImageJ software. The membrane force, axial stretch, and transverse-axial stretch curves in all figures were smoothed using smoothing spline fitting with an R-squared value greater than 0.999. From these smoothed curves, the tangent stiffness and the incremental Poisson's ratio were calculated. The incremental Poisson's ratio is defined here as the negative ratio of increments of the natural logarithms of the stretches in the in-plane transverse and axial directions. The initial stiffness (E_1) and the initial Poisson's ratio (ν_1) were determined as the average values of the tangent stiffness and incremental Poisson's ratio, respectively, in the stretch range from 1.02 to 1.05. The final stiffness (E_2) was calculated as the average value of the tangent stiffness from the stretch value where the derivative of the stiffness first approaches zero to the value as maximum stretch value minus 0.05. The peak Poisson's ratio (ν_2) was defined as the average value of the incremental Poisson's ratio in the stretch range centered around the maximum incremental Poisson's ratio, specifically from the corresponding stretch value minus 0.05 to the value plus 0.05.

Cross-polarization microscope imaging. We prepared the tensile test samples as described in the tensile test methods. For the stretched samples, we stretched them by hand under a dissecting microscope (Zeiss Stemi 508 with Excelis UHD camera), capturing images before and after stretching to calculate the stretch value. The two ends of the sample were then fixed on slides using tape to prevent any further deformation. The samples were imaged at both 0 degrees (stretching direction parallel to the polarizer) and 45 degrees (stretching direction at a 45-degree angle to the polarizer) under a cross-polarization microscope (Olympus BX60 microscope in transmission mode) using a Moticam 10+ camera paired with Motic Image Plus 3.0 software.

Finite element simulations. We imaged the first true leaf from pLH13 (*p35S::mCitrine-RCI2A*) plants with a plasma membrane marker (63) using a Zeiss 710 confocal microscope and obtained the maximum intensity Z projection image. We constructed the cellular structures from the confocal images and stretch them in ABAQUS Standard (2018) as described in SI Methods. The thickness of the cell walls, which was set to 1 µm (64). For comparison, thicknesses of 0.6 µm and 2 µm were also used. Boundary conditions were prescribed as follows: $x = 0$ on boundary AB, $x = 0$ and $y = 0$ on boundary CD, and point D was fixed, and incremental displacement values were applied to the boundaries EF and GH (through defining equation constraints with a reference point R) (Figure S7). Since we were applying a large deformation (maximum stretch was 1.5), we used the neo-Hookean model with Nlgeom (nonlinear geometry) turned on. Additionally, two Yeoh material models with different sets of parameters were used for comparison. The material model parameters are shown in SI Table S1.

ACKNOWLEDGEMENTS

We thank Olivier Hamant for providing *spr2-2* seeds. We thank Alan Zehnder, Sarah Robinson, Virendra Puri, and M Shafayet Zamil for valuable discussions on the design of the micromechanical tensile stage. We thank Karl J. Niklas for insightful discussions on the mechanical behavior of plants. We thank Dorota Kwiatkowska for suggesting the use of fluorescent beads. We thank Catalin Picu for helpful discussions on mechanical behavior and models of fibrous network materials. We thank Lanxi Hu and Ruqiang Zhang for their useful comments on the manuscript. Research reported in this publication was supported by the Engineered Living Materials Institute at Cornell University (SC, BP, MNS), the National Institute Of General Medical Sciences of the National Institutes of Health under Award Number R01GM134037 (IB, AHKR), and the Sam and Nancy Fleming Postdoctoral Fellowship (SC). The authors acknowledge the use of facilities and instrumentation supported by NSF through the Cornell University Materials Research Science and Engineering Center DMR-1719875. The content is solely the responsibility of the authors and does not necessarily represent the official views of the National Institutes of Health.

Bibliography

1. Enrico Coen and Daniel J. Cosgrove. The mechanics of plant morphogenesis. *Science*, 379(6631):eade8055, February 2023. ISSN 0036-8075, 1095-9203. doi: 10.1126/science.ade8055.
2. Duy-Chi Trinh, Juan Alonso-Serra, Mariko Asaoka, Leia Colin, Matthieu Cortes, Alice Malivert, Shogo Takatani, Feng Zhao, Jan Traas, Christophe Trehin, and Olivier Hamant. How Mechanical Forces Shape Plant Organs. *Current Biology*, 31(3):R143–R159, February 2021. ISSN 0960-9822. doi: 10.1016/j.cub.2020.12.001.
3. Kexin Guo, Changjin Huang, Yansong Miao, Daniel J. Cosgrove, and K. Jimmy Hsia. Leaf morphogenesis: The multifaceted roles of mechanics. *Molecular Plant*, 15(7):1098–1119, July 2022. ISSN 1674-2052. doi: 10.1016/j.molp.2022.05.015.
4. Vincent Mirabet, Pradeep Das, Arezki Boudaoud, and Olivier Hamant. The Role of Mechanical Forces in Plant Morphogenesis. *Annual Review of Plant Biology*, 62(1):365–385, 2011. doi: 10.1146/annurev-arplant-042110-103852.
5. Kaare H. Jensen and Yoèel Forterre, editors. *Soft Matter in Plants: From Biophysics to Biomimetics.* Number 15 in Soft Matter Series. Royal Society of Chemistry, London, 2023. ISBN 978-1-78801-724-4.
6. Olivier Hamant, Marcus G. Heisler, Henrik Jönsson, Pawel Krupinski, Magalie Uyttewaal, Plamen Bokov, Francis Corson, Patrik Sahlin, Arezki Boudaoud, Elliot M. Meyerowitz, Yves Couder, and Jan Traas. Developmental Patterning by Mechanical Signals in *Arabidopsis*. *Science*, 322(5908):1650–1655, December 2008. ISSN 0036-8075, 1095-9203. doi: 10.1126/science.1165594.
7. Arun Sampathkumar, An Yan, Pawel Krupinski, and Elliot M. Meyerowitz. Physical forces regulate plant development and morphogenesis. *Current Biology*, 24(10):R475–R483, May 2014. ISSN 0960-9822. doi: 10.1016/j.cub.2014.03.014.
8. James A. Lockhart. An analysis of irreversible plant cell elongation. *Journal of Theoretical Biology*, 8(2):264–275, March 1965. ISSN 0022-5193. doi: 10.1016/0022-5193(65)90077-9.
9. Lincoln Taiz, Eduardo Zeiger, Ian M Møller, and Angus Murphy. *Plant physiology and Development.* Sinauer Associates, Inc, 2015.

10. Daniel J Cosgrove. Building an extensible cell wall. *Plant Physiology*, 189(3):1246–1277, 2022.
11. Robert Kelly-Bellow, Karen Lee, Richard Kennaway, J. Elaine Barclay, Annabel Whibley, Claire Bushell, Jamie Spooner, Man Yu, Paul Brett, Baldeep Kular, Shujing Cheng, Jinfang Chu, Ting Xu, Brendan Lane, James Fitzsimons, Yongbiao Xue, Richard S. Smith, Christopher D. Whitewoods, and Enrico Coen. Brassinosteroid coordinates cell layer interactions in plants via cell wall and tissue mechanics. *Science*, 380(6651):1275–1281, June 2023. doi: 10.1126/science.adf0752.
12. U. Kutschera and K. J. Niklas. The epidermal-growth-control theory of stem elongation: An old and a new perspective. *Journal of Plant Physiology*, 164(11):1395–1409, November 2007. ISSN 0176-1617. doi: 10.1016/j.jplph.2007.08.002.
13. Peter Q. Nguyen, Noémie-Manuelle Dorval Courchesne, Anna Duraj-Thatte, Pichet Praveschotinunt, and Neel S. Joshi. Engineered Living Materials: Prospects and Challenges for Using Biological Systems to Direct the Assembly of Smart Materials. *Advanced Materials*, 30(19):1704847, 2018. ISSN 1521-4095. doi: 10.1002/adma.201704847.
14. Wil V. Srubar. Engineered Living Materials: Taxonomies and Emerging Trends. *Trends in Biotechnology*, 39(6):574–583, June 2021. ISSN 01677799. doi: 10.1016/j.tibtech.2020.10.009.
15. Bolin An, Yanyi Wang, Yuanyuan Huang, Xinyu Wang, Yuzhu Liu, Dongmin Xun, George M. Church, Zhuojun Dai, Xiao Yi, Tzu-Chieh Tang, and Chao Zhong. Engineered Living Materials For Sustainability. *Chemical Reviews*, 123(5):2349–2419, March 2023. ISSN 0009-2665. doi: 10.1021/acs.chemrev.2c00512.
16. Nicholas J. Provart, Jose Alonso, Sarah M. Assmann, Dominique Bergmann, Siobhan M. Brady, Jelena Brkljacic, John Browse, Clint Chapple, Vincent Colot, Sean Cutler, Jeff Dangl, David Ehrhardt, Joanna D. Friesner, Wolf B. Frommer, Erich Grotewold, Elliot Meyerowitz, Jennifer Nemhauser, Magnus Nordborg, Craig Pikaard, John Shanklin, Chris Somerville, Mark Stitt, Keiko U. Torii, Jamie Waese, Doris Wagner, and Peter McCourt. 50 years of Arabidopsis research: Highlights and future directions. *New Phytologist*, 209(3):921–944, 2016. ISSN 1469-8137. doi: 10.1111/nph.13687.
17. Karl J. Niklas and Hanns-Christof Spatz. *Plant Physics*. University of Chicago Press, 2012. ISBN 978-0-226-15081-9 978-0-226-58632-8 978-0-226-58634-2. doi: 10.7208/chicago/9780226586342.001.0001.
18. Amir J Bidhendi and Anja Geitmann. Methods to quantify primary plant cell wall mechanics. *Journal of Experimental Botany*, 70(14):3615–3648, July 2019. ISSN 0022-0957. doi: 10.1093/jxb/erz281.
19. Pascale Milani, Maryam Gholamirad, Jan Traas, Alain Arnéodo, Arezki Boudaoud, Françoise Argoul, and Olivier Hamant. In vivo analysis of local wall stiffness at the shoot apical meristem in arabidopsis using atomic force microscopy. *The Plant Journal*, 67(6):1116–1123, 2011.
20. Tian Zhang, Haosu Tang, Dimitrios Vavylonis, and Daniel J. Cosgrove. Disentangling loosening from softening: Insights into primary cell wall structure. *The Plant Journal*, 100(6):1101–1117, 2019. ISSN 1365-313X. doi: 10.1111/tpj.14519.
21. M. S. Zamil, Hojae Yi, M. A. Haque, and Virendra M. Puri. Characterizing microscale biological samples under tensile loading: Stress–strain behavior of cell wall fragment of onion outer epidermis. *American Journal of Botany*, 100(6):1105–1115, 2013. ISSN 1537-2197. doi: 10.3732/ajb.1200649.
22. M. Shafayet Zamil, Hojae Yi, and Virendra M. Puri. The mechanical properties of plant cell walls soft material at the subcellular scale: The implications of water and of the intercellular boundaries. *Journal of Materials Science*, 50(20):6608–6623, October 2015. ISSN 1573-4803. doi: 10.1007/s10853-015-9204-9.
23. Alexis Peaucelle, Siobhan A Braybrook, Laurent Le Guillou, Emeric Bron, Cris Kuhlemeier, and Herman Höfte. Pectin-induced changes in cell wall mechanics underlie organ initiation in arabidopsis. *Current Biology*, 21(20):1720–1726, 2011.
24. Lilan Hong, Mathilde Dumond, Satoru Tsugawa, Aleksandra Sapala, Anne-Lise Routier-Kierzkowska, Yong Zhou, Catherine Chen, Annamaria Kiss, Mingyuan Zhu, Olivier Hamant, Richard S. Smith, Tamiki Komatsuzaki, Chun-Biu Li, Arezki Boudaoud, and Adrienne H. K. Roeder. Variable Cell Growth Yields Reproducible Organ Development through Spatiotemporal Averaging. *Developmental Cell*, 38(1):15–32, July 2016. ISSN 1534-5807. doi: 10.1016/j.devcel.2016.06.016.
25. Jingyi Yu, Yao Zhang, and Daniel J Cosgrove. The nonlinear mechanics of highly extensible plant epidermal cell walls. *Proceedings of the National Academy of Sciences*, 121(2):e2316396121, 2024.
26. Gabriella Mosca, Aleksandra Sapala, Soeren Strauss, Anne-Lise Routier-Kierzkowska, and Richard S Smith. On the micro-indentation of plant cells in a tissue context. *Physical Biology*, 14(1):015003, 2017.
27. Richard Malgat, François Faure, and Arezki Boudaoud. A mechanical model to interpret cell-scale indentation experiments on plant tissues in terms of cell wall elasticity and turgor pressure. *Frontiers in Plant Science*, 7:1351, 2016.
28. Peter Ryden, Keiko Sugimoto-Shirasu, Andrew Charles Smith, Kim Findlay, Wolf-Dieter Reiter, and Maureen Caroline McCann. Tensile properties of arabidopsis cell walls depend on both a xyloglucan cross-linked microfibrillar network and rhamnogalacturonan ii-borate complexes. *Plant Physiology*, 132(2):1033–1040, 2003.
29. Willie Abasolo, Michaela Eder, Kazuchika Yamauchi, Nicolai Obel, Antje Reinecke, Lutz Neumetzler, John WC Dunlop, Gregory Mouille, Markus Pauly, Herman Höfte, et al. Pectin may hinder the unfolding of xyloglucan chains during cell deformation: implications of the mechanical performance of arabidopsis hypocotyls with pectin alterations. *Molecular Plant*, 2(5):990–999, 2009.
30. Sarah Robinson, Michal Huflejt, Pierre Barbier de Reuille, Siobhan A. Braybrook, Martine Schorderet, Didier Reinhardt, and Cris Kuhlemeier. An Automated Confocal Micro-Extensometer Enables in Vivo Quantification of Mechanical Properties with Cellular Resolution. *The Plant Cell*, 29(12):2959–2973, December 2017. ISSN 1040-4651, 1532-298X. doi: 10.1105/tpc.17.00753.
31. Sarah Robinson and Cris Kuhlemeier. Global Compression Reorients Cortical Microtubules in Arabidopsis Hypocotyl Epidermis and Promotes Growth. *Current Biology*, 28(11):1794–1802.e2, June 2018. ISSN 0960-9822. doi: 10.1016/j.cub.2018.04.028.
32. Amir J. Bidhendi, Hongbo Li, and Anja Geitmann. Modeling the nonlinear elastic behavior of plant epidermis. *Botany*, 98(1):49–64, January 2020. ISSN 1916-2790, 1916-2804. doi: 10.1139/cjb-2019-0058.
33. Bing Pan. Digital image correlation for surface deformation measurement: historical developments, recent advances and future goals. *Measurement Science and Technology*, 29(8):082001, 2018.
34. Joanna Elsner, Marcin Lipowczan, and Dorota Kwiatkowska. Differential growth of pavement cells of arabidopsis thaliana leaf epidermis as revealed by microbead labeling. *American journal of botany*, 105(2):257–265, 2018.
35. Yael Abraham and Rivka Elbaum. Quantification of microfibril angle in secondary cell walls at subcellular resolution by means of polarized light microscopy. *New Phytologist*, 197(3):1012–1019, 2013.
36. Chase P Broedersz and Fred C MacKintosh. Modeling semiflexible polymer networks. *Reviews of Modern Physics*, 86(3):995–1036, 2014.
37. Jingyi Yu, Joshua T Del Mundo, Guillaume Freychet, Mikhail Zhernenkov, Eric Schaible, Esther W Gomez, Enrique D Gomez, and Daniel J Cosgrove. Dynamic structural change of plant epidermal cell walls under strain. *Small*, page 2311832, 2024.
38. Catalin R Picu. Network materials: structure and properties. 2022.
39. N Parvez, J Merson, and RC Picu. Stiffening mechanisms in stochastic athermal fiber networks. *Physical Review E*, 108(4):044502, 2023.
40. Pascale Milani, Vincent Mirabet, Coralie Cellier, Frédérique Rozier, Olivier Hamant, Pradeep Das, and Arezki Boudaoud. Matching patterns of gene expression to mechanical stiffness at cell resolution through quantitative tandem epifluorescence and nanoindentation. *Plant Physiology*, 165(4):1399–1408, 2014.
41. Olivier Hamant, Daisuke Inoue, David Bouchez, Jacques Dumais, and Eric Mjolsness. Are microtubules tension sensors? *Nature Communications*, 10(1):2360, May 2019. ISSN 2041-1723. doi: 10.1038/s41467-019-10207-y.
42. Tsubasa Shoji, Noriyuki N. Narita, Kazunori Hayashi, Junko Asada, Takahiro Hamada, Seiji Sonobe, Keiji Nakajima, and Takashi Hashimoto. Plant-Specific Microtubule-Associated Protein SPIRAL2 Is Required for Anisotropic Growth in Arabidopsis. *Plant Physiology*, 136(4):3933–3944, December 2004. ISSN 0032-0889. doi: 10.1104/pp.104.051748.
43. Raymond Wightman, Guillaume Chomicki, Manoj Kumar, Paul Carr, and Simon R Turner. Spiral2 determines plant microtubule organization by modulating microtubule severing. *Current Biology*, 23(19):1902–1907, 2013.
44. Yuanwei Fan, Graham M. Burkart, and Ram Dixit. The Arabidopsis SPIRAL2 Protein Targets and Stabilizes Microtubule Minus Ends. *Current Biology*, 28(6):987–994.e3, March 2018. ISSN 0960-9822. doi: 10.1016/j.cub.2018.02.014.
45. Nathan Hervieux, Mathilde Dumond, Aleksandra Sapala, Anne-Lise Routier-Kierzkowska, Daniel Kierzkowski, Adrienne HK Roeder, Richard S Smith, Arezki Boudaoud, and Olivier Hamant. A mechanical feedback restricts sepal growth and shape in arabidopsis. *Current Biology*, 26(8):1019–1028, 2016.
46. Gerhard A Holzapfel et al. Biomechanics of soft tissue. *The handbook of materials behavior models*, 3(1):1049–1063, 2001.
47. Steven Vogel. *Comparative biomechanics: life's physical world*. Princeton University Press, 2013.
48. RS Gates, RE Pitt, A Ruina, and JR Cooke. Cell wall elastic constitutive laws and stress-strain behavior of plant vegetative tissue. *Biorheology*, 23(5):453–466, 1986.
49. M. L. Oey, E. Vanstreels, J. De Baerdemaeker, E. Tijskens, H. Ramon, M. L. A. T. M. Hertog, and B. Nicolaï. Effect of turgor on micromechanical and structural properties of apple tissue: A quantitative analysis. *Postharvest Biology and Technology*, 44(3):240–247, June 2007. ISSN 0925-5214. doi: 10.1016/j.postharvbio.2006.12.015.
50. Daniel Kierzkowski, Naomi Nakayama, Anne-Lise Routier-Kierzkowska, Alain Weber, Emmanuelle Bayer, Martine Schorderet, Didier Reinhardt, Cris Kuhlemeier, and Richard S. Smith. Elastic Domains Regulate Growth and Organogenesis in the Plant Shoot Apical Meristem. *Science*, 335(6072):1096–1099, March 2012. doi: 10.1126/science.1213100.
51. Catalin R Picu. Constitutive models for random fiber network materials: a review of current status and challenges. *Mechanics Research Communications*, 114:103605, 2021.
52. Qinghua Meng and Yuan Gao. On the strain stiffening and nanofiber orientation of physically crosslinked nanocellulose hydrogels. *International Journal of Solids and Structures*, 276:112325, 2023.
53. Yuli Chen, Yong Ma, Qifang Yin, Fei Pan, Chaojie Cui, Zuoqi Zhang, and Bin Liu. Advances in mechanics of hierarchical composite materials. *Composites Science and Technology*, 214:108970, 2021.
54. Meredith N. Silberstein, Chia-Ling Pai, Gregory C. Rutledge, and Mary C. Boyce. Elastic–plastic behavior of non-woven fibrous mats. *Journal of the Mechanics and Physics of Solids*, 60(2):295–318, February 2012. ISSN 00225096. doi: 10.1016/j.jmps.2011.10.007.
55. Mohammad Retaful Islam, Gregory Tudryn, R Bucinell, L Schadler, and RC Picu. Morphology and mechanics of fungal mycelium. *Scientific reports*, 7(1):13070, 2017.
56. Valerie Tutwiler, Jaspreet Singh, Rustem I Litvinov, John L Bassani, Prashant K Purohit, and John W Weisel. Rupture of blood clots: Mechanics and pathophysiology. *Science advances*, 6(35):eabc0496, 2020.
57. Stéphane Bancelin, Barbara Lynch, Christelle Bonod-Bidaud, Guillaume Ducourthial, Sotiris Psilodimitrakopoulos, Petr Dokládal, Jean-Marc Allain, Marie-Claire Schanne-Klein, and Florence Ruggiero. Ex vivo multiscale quantitation of skin biomechanics in wild-type and genetically-modified mice using multiphoton microscopy. *Scientific reports*, 5(1):17635, 2015.
58. Yuan-Cheng Fung. *Biomechanics: mechanical properties of living tissues*. Springer Science & Business Media, 2013.
59. Andrei Pissarenko, Wen Yang, Haocheng Quan, Katherine A Brown, Alun Williams, William G Proud, and Marc A Meyers. Tensile behavior and structural characterization of pig dermis. *Acta biomaterialia*, 86:77–95, 2019.
60. Jessica WY Jor, Martyn P Nash, Poul MF Nielsen, and Peter J Hunter. Estimating material parameters of a structurally based constitutive relation for skin mechanics. *Biomechanics and modeling in mechanobiology*, 10:767–778, 2011.
61. Daniel J. Cosgrove. Structure and growth of plant cell walls. *Nature Reviews Molecular Cell Biology*, 25(5):340–358, May 2024. ISSN 1471-0072, 1471-0080. doi: 10.1038/s41580-023-00691-y.

62. Yao Zhang, Jingyi Yu, Xuan Wang, Daniel M. Durachko, Sulin Zhang, and Daniel J. Cosgrove. Molecular insights into the complex mechanics of plant epidermal cell walls. *Science*, 372(6543):706–711, May 2021. doi: 10.1126/science.abf2824.
63. Dana O Robinson, Jeremy E Coate, Abhyudai Singh, Lilan Hong, Max Bush, Jeff J Doyle, and Adrienne HK Roeder. Ploidy and size at multiple scales in the arabidopsis sepal. *The Plant Cell*, 30(10):2308–2329, 2018.
64. Elham Forouzesh, Ashwani Goel, Sally A Mackenzie, and Joseph A Turner. In vivo extraction of arabidopsis cell turgor pressure using nanoindentation in conjunction with finite element modeling. *The Plant Journal*, 73(3):509–520, 2013.